Identification and mapping of dikes with relatively primitive compositions in Thaumasia Planum on Mars: Implications for Tharsis volcanism and the opening of Valles Marineris

Jun Huang,[1,2] Christopher S. Edwards,[2] Briony H. N. Horgan,[2] Philip R. Christensen,[2] Michael D. Kraft,[2] and Long Xiao[1]

Received 31 May 2012; revised 27 July 2012; accepted 28 July 2012; published 6 September 2012.

[1] We have identified several exposed dikes in Thaumasia Planum Mars using THEMIS, CTX, HiRISE and CRISM data. These dikes extend from tens to ~100 kilometers in length with average widths of ~50 m. They display classic 'en echelon' patterns while cross-cutting preexisting geologic features, including extensive wrinkle ridges. Both the dikes and associated fissure eruption products have very blocky morphologies with ~38% higher thermal inertia than the surrounding regions. The dikes are all enriched in Mg-rich olivine relative to surrounding terrain, and a subset also contains elevated high-calcium pyroxene, both of which indicate relatively primitive magma compositions. We propose that these dikes might have served as feeders for the olivine-enriched flood basalts in this region, and may be derived from the Tharsis plume. These observations provide further evidence that the opening of Valles Marineris was facilitated by tectonic stresses following paths of preferential weakness along preexisting structures such as fractures and faults like those indicated by these dikes. **Citation:** Huang, J., C. S. Edwards, B. H. N. Horgan, P. R. Christensen, M. D. Kraft, and L. Xiao (2012), Identification and mapping of dikes with relatively primitive compositions in Thaumasia Planum on Mars: Implications for Tharsis volcanism and the opening of Valles Marineris, *Geophys. Res. Lett.*, *39*, L17201, doi:10.1029/2012GL052523.

1. Introduction

[2] Dikes are igneous intrusions into pre-existing rocks, and are in-place records of volcanism that can provide fundamental geologic information about terrestrial planets. Although Mars is largely a volcanic planet [*Greeley and Spudis*, 1981; *Werner*, 2009; *Xiao et al.*, 2012], dikes are rarely exposed at the surface likely due to the lack of tectonic uplift and low erosion rates, which are processes important for exposing subsurface dikes on Earth [*Ernst et al.*, 2001; *Pedersen et al.*, 2010]. Dikes may be inferred from associated surface morphologies including pit craters, narrow grabens, linear and ovoid troughs [*Mège and Masson*, 1996; *Wilson and Head*, 2002; *Mège et al.*, 2003; *Schultz et al.*, 2004] and magnetic anomalies [*Nimmo*, 2000]. Recently, several direct observations of eroded and exposed dikes, including some with unique compositions have been reported on Mars [*Shean et al.*, 2005; *Head et al.*, 2006; *Korteniemi et al.*, 2010; *Pedersen et al.*, 2010; *Flahaut et al.*, 2011]. Here, we report new observations of dikes in Thaumasia Planum (Figure 1a) using imaging and spectral data from THEMIS (Thermal Emission Imaging System) [*Christensen et al.*, 2004], CTX (Context Camera) [*Malin et al.*, 2007], HiRISE (High Resolution Imaging Science Experiment) [*McEwen et al.*, 2007] and CRISM (Compact Reconnaissance Imaging Spectrometer for Mars) [*Murchie et al.*, 2007]. The region in which these dikes occur is characterized by extensive sinuous wrinkle ridges and has been previously mapped as Older Ridged Plains Material (HNr) of Late Noachian to Early Hesperian age [*Dohm et al.*, 2001]. The dikes we identified are thermophysically and compositionally distinct from the surrounding terrains and constrain the volcanic history related to early Tharsis uplift and opening of Valles Marineris.

2. Methods

[3] We used the 100 m/pixel THEMIS daytime infrared (IR) global mosaic [*Edwards et al.*, 2011] to survey the region of Thaumasia Planum (21–27°S, 291–300°E). The mosaic highlights relative daytime surface temperatures, which vary due to solar illumination and material grain-size [e.g., *Fergason et al.*, 2006]. Therefore, we used this dataset to distinguish different geologic materials and to establish regional context. Using THEMIS nighttime IR data converted to thermal inertia [*Fergason et al.*, 2006] we derived the thermophysical nature of the materials. We further characterized morphologic features in detail using CTX and HiRISE images (~6 m/pixel and ~25–30 cm/pixel, respectively). The OLINDEX [*Pelkey et al.*, 2007] spectral index was calculated for CRISM multispectral survey (MSP) data (~200 m/pixel in 72 selected channels) to investigate regional compositions. We calculated the OLINDEX2 [*Salvatore et al.*, 2010], LCPINDEX and HCPINDEX [*Pelkey et al.*, 2007] spectral indices for full resolution targeted (FRT) data in order to map locations with enhancements in olivine, low- and high-calcium pyroxene, respectively. FRT data were used to estimate the Lambert albedo from both the visible/near infrared (VNIR) and IR detectors (700–2400 nm) [*Murchie et al.*, 2007]. In order to account for slight differences in viewing geometry between the VNIR and IR detectors, the VNIR portion of both spectra have been multiplied by a constant to

[1]Planetary Science Institute, Faculty of Earth Sciences, China University of Geosciences, Wuhan, Hubei, China.
[2]Mars Space Flight Facility, School of Earth and Space Exploration, Arizona State University, Tempe, Arizona, USA.

Corresponding author: J. Huang, Planetary Science Institute, Faculty of Earth Sciences, China University of Geosciences, Wuhan, Hubei 430074, China. (jhuang.cug@gmail.com)

0094-8276/12/2012GL052523

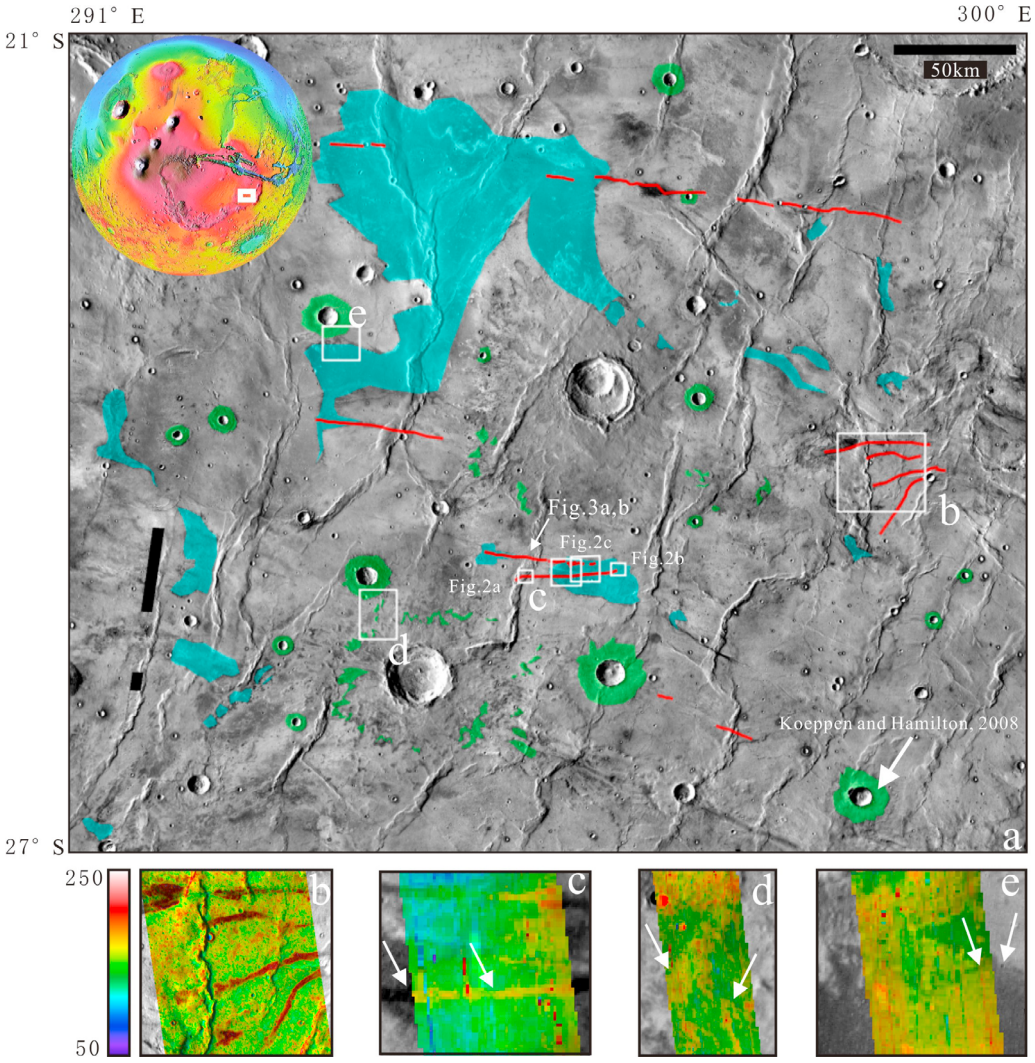

Figure 1. (a) THEMIS daytime infrared temperature mosaic (background) of the study area (27°–21°S and 291–300°E). Colored features are the identified olivine-enriched and higher thermal inertia regions: red lines are linear features; green polygons are ejecta of impact craters; blue shapes are rough terrains. The location of olivine (Fo_{68}) concentration derived from TES spectra [*Koeppen and Hamilton*, 2008] is identified by the white arrow. (b) A close-up view of linear features with colorized thermal inertia image (units: $JK^{-1}\ m^{-2}\ s^{-1/2}$, THEMIS nighttime image ID: I06213011) overlain on a THEMIS daytime infrared temperature mosaic. The cold tones indicate a lower thermal inertia and the warm tones indicate a higher thermal inertia. Close-up views of linear features, ejecta of impact craters and rough terrains with colorized OLINDEX index (derived from CRISM MSP data): (c) MSP0000C6EE_01_IF211L_TRR3 and (d and e) MSP00004969_05_IF214L_TRR3) overlain on THEMIS daytime infrared temperature mosaic. Green tones indicate lower olivine concentrations, while red tones indicate higher olivine concentrations. In Figure 1c white arrows indicate the linear features with elevated olivine concentration; in Figure 1d white arrows indicate ejecta of impact craters with elevated olivine concentration; in Figure 1e white arrows indicate rough terrains with elevated olivine concentration.

visually match the albedo of the IR portion [*Horgan and Bell*, 2012].

3. Results

[4] We observe several narrow linear features in the THEMIS daytime IR data in the Thaumasia Planum region (Figure 1a) that display a general east to west trend and are roughly parallel to the orientation of the Valles Marineris. Some features are discontinuous but can be traced for distances up to ~100 km. The linear feature materials are cool relative to the surrounding plains in the daytime images and relatively warm in nighttime images (Figures 1b and 1c). The width of the thermally-distinct zone ranges from ~1–4 km. These materials have thermal inertias of ~220–240 $JK^{-1}\ m^{-2}\ s^{-1/2}$, while the surrounding wrinkle ridges and lava plains have a typical thermal inertia of ~160 $JK^{-1}\ m^{-2}\ s^{-1/2}$.

[5] High-resolution CTX and HiRISE data illustrate small-scale morphologies associated with these linear features (Figure 2). They cross-cut wrinkles ridges and are commonly composed of a sharp-crested ridge ~50 m wide in the center of a topographically lower band of flank material (Figure 2a). In many places, linear features occur as segments ~10–1,000 m long, with some segments occurring 'en echelon' to one another (Figure 2c). On one linear feature, the height of

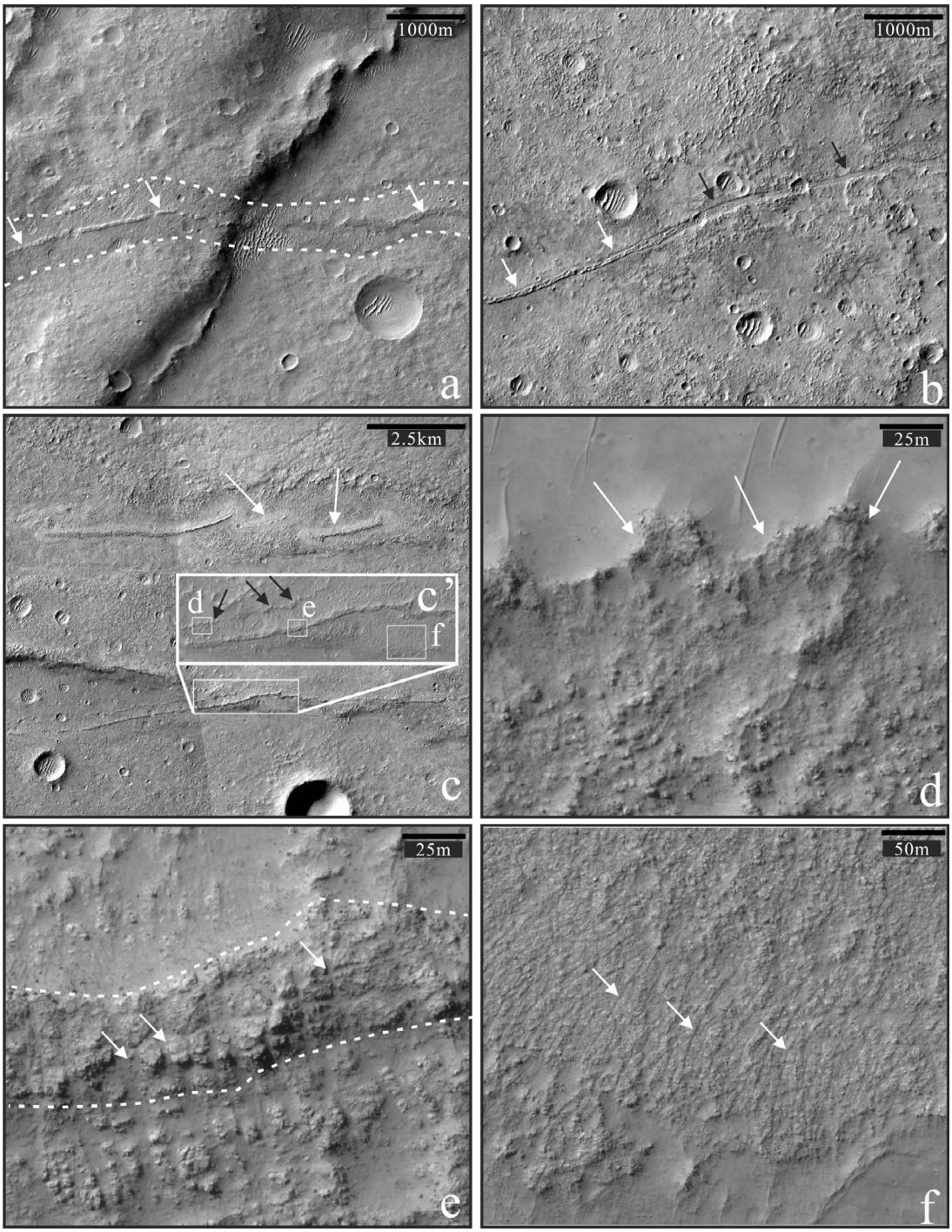

Figure 2. Morphology of the linear features using (a–c) CTX P18_008115_1561_XN_23S066W, B01_010185_1556_XI_24S065W, P17_007759_1547_XI_25S065W) and (d–f) HiRISE (PSP_007759_1550) images. In Figure 2a, a linear feature is observed to cut through a wrinkle ridge. A slightly sinuous ridge (white arrows) is located in the center of the flank materials (white dash lines). Sand dunes are present in regional depressions. As the linear feature extends to the east (Figure 2b), the flank materials disappear and the central ridge (white arrows) transforms to a trough (black arrows) gradually. In Figure 2c, some segments show 'en echelon' pattern (white arrows); the inset c' is a close-up view of another linear feature. In addition to the morphologies shown in Figure 2a, an outer ridge (black arrows) parallel to the central ridge can be seen. Detailed morphology of the outer ridge, the central ridge and the flank materials are presented in Figures 2d, 2e and 2f, respectively. Figure 2d is a close-up view of the outer ridge (white arrows). From this image, it appears rocky and is elevated with respect to the southern rocky flank materials and the northern dusty and rippled terrains. Figure 2e is a close-up view of the central ridge (white dash lines), which appears rockier than the flank materials (shown in Figure 2d). Dozens of near N-S fractures are indicated by white arrows and regional depressions appear to be mantled. Figures 2f is a close-up view of flank materials where hundreds of slightly curved narrow linear troughs (white arrows) can be observed.

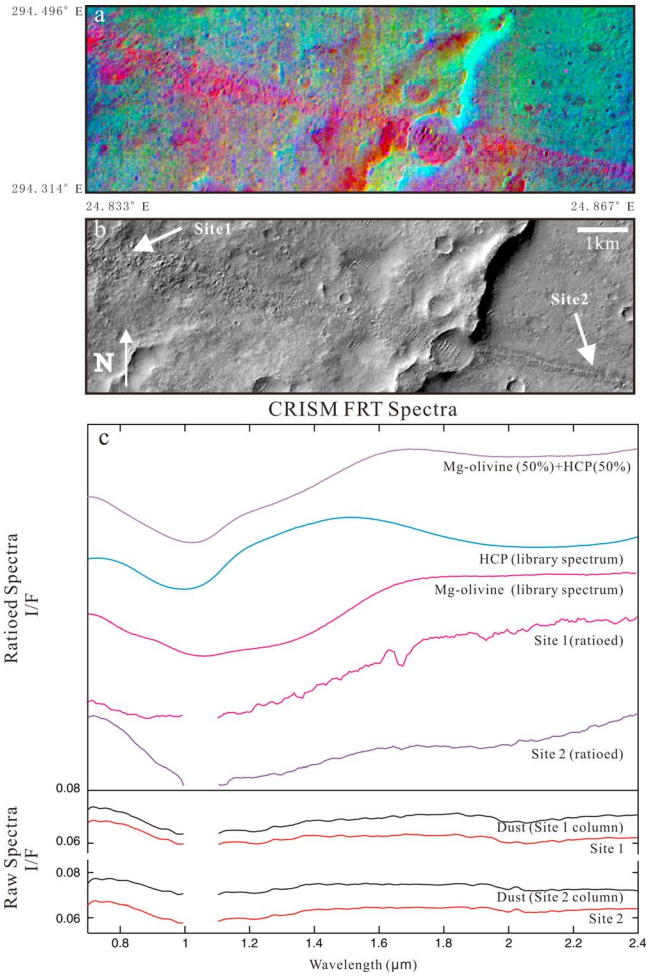

Figure 3. Spectral analysis on CRISM FRT0000AC9F. (a) RGB composition of summary parameters (R: OLINDEX2; G = LCPINDEX; B = HCPINDEX). The variations in the red (olivine) and purple (olivine and HCP) colors along the extent of the linear feature suggest compositional variations, whereas the surrounding terrains show green and blue colors suggestive of pyroxene. (b) CTX image (B01_009974_1548_XI_25S065W) shows the same area as Figure 3a. White arrows indicate the locations of extracted CRISM spectra (Spectra locations of FRT data: Site 1: on the dike: 3 × 3, upper left (UL):(599, 340), dust: 3 × 3, UL:(599, 222); Site 2: on the dike: 9 × 11, UL:(173, 228), dust: 9 × 11, UL:(173, 16)). (c) Two examples of both CRISM raw and ratioed spectra (divided by a dusty area within the same column) over a linear feature. Library spectra are shown for comparison (CRISM spectral library and USGS Digital Spectral Library splib06a).

the central ridge decreases eastward, and it transitions into a trough with no visible flank material (Figure 2b). In some locations, smaller outer ridges run parallel to the central ridge, and they are lower in elevation than the central ridge (Figure 2c; see inset). However, we were unable to derive the topographic information from MOLA gridded data due to the small size of these features (tens of meters) relative to the size of a single MOLA pixel from the 128 ppd map (~400 m/pixel at this latitude). Furthermore, there were no available CTX or HiRISE stereo-image pairs, which would have sufficient resolution to decipher topographic information, over any of these sites.

[6] The outer ridge appears to be composed largely of blocky material and the terrain outside is relatively smooth and partly covered by sand dunes (Figure 2d). Most of the central ridge has a blocky appearance, although some portions are smoother and appear to be mantled by regolith or aeolian material. Linear fractures perpendicular to the orientation of the central ridge (Figure 2e) and extensive small troughs several meters wide within the flank material are observed (Figure 2f).

[7] Many of the linear features in the region have stronger olivine spectral features observed in CRISM MSP OLINDEX parameter maps (Figure 1c). In addition, the ejecta of some impact craters (Figures 1d and 1e) and rougher terrains (Figure 1e) also have elevated OLINDEX values. Similar to the linear features, these surfaces also display a relatively high thermal inertia. Notably, smaller craters' ejecta and the larger craters' outmost ejecta have these characteristics (Figure 1a).

[8] Surface mineralogy was examined in detail for one linear feature, which cuts through the plains and a wrinkle ridge. To investigate the mineralogy of the linear feature we used a red/green/blue (RGB) composite decorrelation stretch image [*Gillespie et al.*, 1986] where the CRISM OLINDEX2, LCPINDEX and HCPINDEX are displayed in the RGB channels respectively (Figure 3a). Based on this false color image, it is apparent that the linear feature has a higher olivine concentration, while the plains and wrinkle ridge have higher LCP and HCP values. The composition of the linear feature varies from primarily olivine-bearing materials (red) to a mixture of olivine and pyroxene (purple) (Figure 3a). Spectra extracted from two locations along the linear feature (Figure 3b) were ratioed to a mean spectrum of a dustier region in the same CRISM column in order to suppress atmospheric components. The ratioed spectra show a broad absorption centered between 1.0–1.1 μm, consistent with iron-bearing silicate minerals (Figure 3c). The spectrum from the red region in Figure 3a has additional absorptions at short wavelengths but no major absorptions beyond 1.5 μm, consistent with olivine [e.g., *Adams*, 1974]. The lack of a strong absorption between 1.2–1.4 μm indicates the olivine composition may be more Mg-rich (forsteritic) than Fe-rich (fayalitic) [*Flahaut et al.*, 2011]. In contrast, the spectrum from the purple region exhibits an additional broad absorption centered near 2 μm, consistent with pyroxene [*Adams*, 1974]. However, the purple spectrum lacks an absorption feature between 0.8–1.0 μm, indicating that the ferrous phase is not LCP. Instead, this spectrum is most consistent with a mixture of olivine and HCP, with an absorption centered near 2.1 μm due to the presence of HCP, and an asymmetry of the 1 μm band skewed toward longer wavelengths due to olivine.

4. Discussion

[9] We interpret the central ridges of these linear features to be dikes based on their: 1) linearity over long distances; 2) diagnostic 'en echelon' patterns; 3) parallel orientation to regional extensional features; 4) blocky morphology with elevated thermal inertia; and 5) igneous composition.

[10] In typical terrestrial examples, the top of a dike rises near to the surface and stops at depth below the surface, generally meters to hundreds of meters depending on local

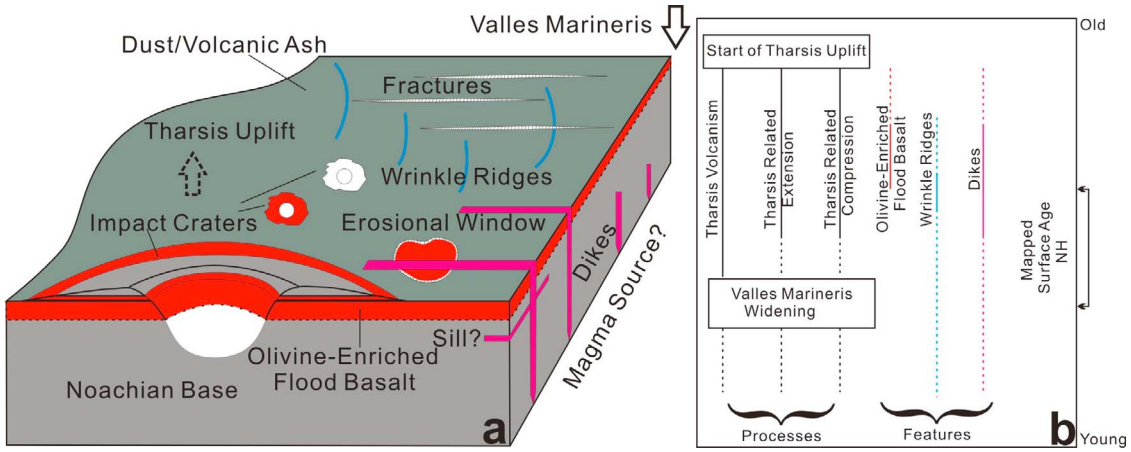

Figure 4. (a) Conceptual diagram showing stratigraphic relationships between observed features (not to scale). (b) Qualitative chronology of observed features and regional processes. Olivine basaltic volcanism is constrained by the start of the Tharsis Rise and the opening of Valles Marineris.

geological conditions [e.g., *Mastin and Pollard*, 1988; *Rubin*, 1992]. These segments may leave narrow troughs with no infilling lavas (Figure 2b). Alternatively, a section of the dike may make its way to the surface, creating a fissure eruption that deposits material adjacent to the dike [e.g., *Wilson and Head*, 1988]. It is possible that the flank features, which exhibit flow-like textures (Figure 2f), are the products of a fissure eruption and the outer ridge may be the lava flow front (Figure 2d).

[11] Surfaces of high thermal inertia are composed of coarser sand and rock fragments, while surfaces of fine particles have a lower thermal inertia. A given thermal inertia can be the result of mixing of different materials [*Christensen*, 1982]. The thermal inertia of the ridges are $\sim$60 JK^{-1} m^{-2} $s^{-1/2}$ higher than that of the surrounding terrains indicating generally coarser materials on the ridges. However, the flank materials, the central ridge, and outer ridge are composed of very blocky materials and finer mantle materials can be observed in low topographic areas (Figures 2d–2f). Limited by the 100 m/pix spatial resolution of THEMIS IR data, we interpret the thermal inertias as a combination of both rocky (>1200 JK^{-1} m^{-2} $s^{-1/2}$) and finer aeolian mantling materials (<100 JK^{-1} m^{-2} $s^{-1/2}$). The result is a bulk thermal inertia significantly lower than bedrock [>1200 JK^{-1} m^{-2} $s^{-1/2}$: *Edwards et al.*, 2009], despite the observations of in-place rock in the HiRISE images (Figures 2d and 2e).

[12] The CRISM ratio spectra from the dike materials indicate Mg-rich olivine as compared to Fe-rich olivine identified in Valles Marineris [*Flahaut et al.*, 2011], and this Mg-enriched composition indicates a relatively primitive magmatic composition [*McSween et al.*, 2006]. Although the dikes are too small to directly obtain quantitative mineralogy using Thermal Emission Spectrometer (TES) data (spatial resolution 3 $\times$ 8 km [*Christensen et al.*, 2001]), the highest model concentrations of Fo_{68} olivine within the wrinkle ridged plain and impact ejecta are $\sim$20% using the maps from *Koeppen and Hamilton* [2008]. The concentrations of Mg-rich olivine in the dikes are likely $\sim$20% based on the assumption of compositional similarity.

[13] The occurrence of olivine in the smaller and larger craters' outmost ejecta (Figures 1a, 1d, and 1e) is consistent with a near-surface and shallow olivine deposit based on observations of both terrestrial and Martian craters [*Osinski et al.*, 2011]. However, not all the ejecta exhibit this characteristic, so the subsurface layer may be discontinuous or may lie below the depth sampled by the smaller craters. Lateral variations in ejecta composition reflect vertical differences in the target materials and indicate that the subsurface layer is relatively thin (<$\sim$400 m based on the depths of impact craters). We propose that the higher thermal inertia and olivine-enriched ejecta materials are windows into the subsurface of the wrinkle ridged plains.

[14] Based on the observations and discussion above, we propose a scenario for geological evolution of the region, which is summarized schematically in Figure 4: First the regional stress field was set with radial extension and tangential compression in Thaumasia Planum due to Tharsis load [*Andrews-Hanna*, 2012a]. Next the mantle derived olivine-enriched flood basalts were emplaced over the Noachian basement rock. Then extensive wrinkle ridges formed due to regional compression [*Golombek et al.*, 2001]. As dikes often spread laterally within pre-existing strata on Earth [*Ray et al.*, 2007], the dike system (including the dikes in this study and those identified by *Flahaut et al.* [2011]) may have been the source conduits for magma to feed the lava flows (supported by the compositional similarity). Finally, dust and/or volcanic ash covered the region, and along with impact and aeolian processes, masked the olivine signatures of the surface. This scenario is consistent with regional extension in Thaumasia Planum resulting from Tharsis loading upon the dichotomy boundary [*Andrews-Hanna et al.*, 2012a]. The dikes we observed in Thaumasia Planum are likely related to dikes in Valles Marineris that are thought to have contributed significantly to subsidence of the Valles Marineris [*Andrews-Hanna*, 2012a, 2012b].

[15] The emplacement of more mafic, rockier dikes in this region has implications for magmatic history of Mars. No direct source of magma has been identified in this region, but given the general proximity to the Tharsis volcanic province, it is plausible that the dikes were sourced from the

Tharsis plume. Additionally, given that the extension directions of the dikes are roughly parallel to Valles Marineris, it is also plausible that the fractures associated with Valles Marineris provided the path for dike emplacement. Therefore, we propose that the relatively primitive magmas of Tharsis volcanism may have traveled along pre-existing fracture systems and formed both the Thaumasia Planum dikes and flood basalts.

5. Conclusion

[16] We have identified several linear features in Thaumasia Planum Mars consistent with an interpretation as igneous dikes. They are associated with fissure eruptions, are composed of blocky material, and have relatively higher thermal inertia than nearby regions. They vary compositionally from predominantly forsteritic olivine-bearing materials to materials that contain both forsteritic olivine and pyroxene signatures. The forsteritic composition of the dikes indicates that they are likely sourced from a primitive mantle. Based on the results of our study, the dikes identified here likely fed olivine-enriched flood basalts in Thaumasia Planum. Dike orientations indicate they are directly associated with the Tharsis-related stress field that formed the Valles Marineris, and the relatively olivine-rich, primitive composition of dikes are consistent with a mantle source, perhaps directly related to a Tharsis mantle plume.

[17] **Acknowledgments.** This study was supported by the Natural Science Foundation of China (41072045) and the National Basic Research Program of China (2010CB808906). All the figures are generated by JMARS (http://jmars.asu.edu/) and Davinci (http://davinci.asu.edu/). We thank Mikki Osterloo and Livio Tornabene for their thorough reviews that greatly improved the manuscript. Dale Noss, Saadat Anwar and Scott Dickenshied assisted data process. Amanda Clark, Andy Ryan and Steve Ruff provided insight suggestions. Additionally, we thank Robin Fergason who kindly provided the thermal inertia data.

[18] The Editor thanks Mikki Osterloo and an anonymous reviewer for their assistance evaluating this paper.

References

Adams, J. B. (1974), Visible and near-infrared diffuse reflectance spectra of pyroxenes as applied to remote sensing of solid objects in the solar system, *J. Geophys. Res.*, *79*(32), 4829–4836, doi:10.1029/JB079i032p04829.

Andrews-Hanna, J. C. (2012a), The formation of Valles Marineris: 2. Stress focusing along the buried dichotomy boundary, *J. Geophys. Res.*, *117*, E04009, doi:10.1029/2011JE003954.

Andrews-Hanna, J. C. (2012b), The formation of Valles Marineris: 3. Trough formation through super-isostasy, stress, sedimentation, and subsidence, *J. Geophys. Res.*, *117*, E06002, doi:10.1029/2012JE004059.

Christensen, P. R. (1982), Martian dust mantling and surface composition: Interpretation of thermophysical properties, *J. Geophys. Res.*, *87*(B12), 9985–9998, doi:10.1029/JB087iB12p09985.

Christensen, P. R., et al. (2001), Mars Global Surveyor Thermal Emission Spectrometer experiment: Investigation description and surface science results, *J. Geophys. Res.*, *106*(E10), 23,823–23,871, doi:10.1029/2000JE001370.

Christensen, P. R., et al. (2004), The Thermal Emission Imaging System (THEMIS) for the Mars 2001 Odyssey mission, *Space Sci. Rev.*, *110*(1), 85–130, doi:10.1023/B:SPAC.0000021008.16305.94.

Dohm, J. M., et al. (2001), Geological map of the Thaumasia region, *U.S. Geol. Surv. Geol. Invest. Map Ser.*, *I-2650*.

Edwards, C. S., J. L. Bandfield, P. R. Christensen, and R. L. Fergason (2009), Global distribution of bedrock exposures on Mars using THEMIS high-resolution thermal inertia, *J. Geophys. Res.*, *114*, E11001, doi:10.1029/2009JE003363.

Edwards, C. S., P. R. Christensen, and J. Hill (2011), Mosaicking of global planetary image datasets: 2. Modeling of wind streak thicknesses observed in Thermal Emission Imaging System (THEMIS) daytime and nighttime infrared data, *J. Geophys. Res.*, *116*, E10005, doi:10.1029/2011JE003857.

Ernst, R. E., et al. (2001), Giant dike swarms: Earth, Venus, and Mars, *Annu. Rev. Earth Planet. Sci.*, *29*, 489–534, doi:10.1146/annurev.earth.29.1.489.

Fergason, R. L., P. R. Christensen, and H. H. Kieffer (2006), High-resolution thermal inertia derived from the Thermal Emission Imaging System (THEMIS): Thermal model and applications, *J. Geophys. Res.*, *111*, E12004, doi:10.1029/2006JE002735.

Flahaut, J., J. F. Mustard, C. Quantin, H. Clenet, P. Allemand, and P. Thomas (2011), Dikes of distinct composition intruded into Noachian-aged crust exposed in the walls of Valles Marineris, *Geophys. Res. Lett.*, *38*, L15202, doi:10.1029/2011GL048109.

Gillespie, A. R., et al. (1986), Color enhancement of highly correlated images. 1. decorrelation and HSI contrast stretches, *Remote Sens. Environ.*, *20*(3), 209–235, doi:10.1016/0034-4257(86)90044-1.

Golombek, M. P., F. S. Anderson, and M. T. Zuber (2001), Martian wrinkle ridge topography: Evidence for subsurface faults from MOLA, *J. Geophys. Res.*, *106*(E10), 23,811–23,821, doi:10.1029/2000JE001308.

Greeley, R., and P. D. Spudis (1981), Volcanism on Mars, *Rev. Geophys.*, *19*(1), 13–41, doi:10.1029/RG019i001p00013.

Head, J. W., et al. (2006), The Huygens-Hellas giant dike system on Mars: Implications for late Noachian–early Hesperian volcanic resurfacing and climatic evolution, *Geology*, *34*(4), 285–288, doi:10.1130/G22163.1.

Horgan, B., and J. F. Bell (2012), Widespread weathered glass on the surface of Mars, *Geology*, *40*(5), 391–394, doi:10.1130/G32755.1.

Koeppen, W. C., and V. E. Hamilton (2008), Global distribution, composition, and abundance of olivine on the surface of Mars from thermal infrared data, *J. Geophys. Res.*, *113*, E05001, doi:10.1029/2007JE002984.

Korteniemi, J., et al. (2010), Dike indicators in the Hadriaca Patera–Promethei Terra region, Mars, *Earth Planet. Sci. Lett.*, *294*(3–4), 466–478, doi:10.1016/j.epsl.2009.06.038.

Malin, M. C., et al. (2007), Context Camera Investigation on board the Mars Reconnaissance Orbiter, *J. Geophys. Res.*, *112*, E05S04, doi:10.1029/2006JE002808.

Mastin, L. G., and D. D. Pollard (1988), Surface deformation and shallow dike intrusion processes at Inyo Craters, Long Valley, California, *J. Geophys. Res.*, *93*(B11), 13,221–13,235, doi:10.1029/JB093iB11p13221.

McEwen, A. S., et al. (2007), Mars Reconnaissance Orbiter's High Resolution Imaging Science Experiment (HiRISE), *J. Geophys. Res.*, *112*, E05S02, doi:10.1029/2005JE002605.

McSween, H. Y., et al. (2006), Characterization and petrologic interpretation of olivine-rich basalts at Gusev Crater, Mars, *J. Geophys. Res.*, *111*, E02S10, doi:10.1029/2005JE002477.

Mège, D., and P. Masson (1996), A plume tectonics model for the Tharsis province, Mars, *Planet. Space Sci.*, *44*(12), 1499–1546, doi:10.1016/S0032-0633(96)00113-4.

Mège, D., A. C. Cook, E. Garel, Y. Lagabrielle, and M.-H. Cormier (2003), Volcanic rifting at Martian grabens, *J. Geophys. Res.*, *108*(E5), 5044, doi:10.1029/2002JE001852.

Murchie, S., et al. (2007), Compact reconnaissance Imaging Spectrometer for Mars (CRISM) on Mars Reconnaissance Orbiter (MRO), *J. Geophys. Res.*, *112*, E05S03, doi:10.1029/2006JE002682.

Nimmo, F. (2000), Dike intrusion as a possible cause of linear Martian magnetic anomalies, *Geology*, *28*(5), 391–394, doi:10.1130/0091-7613(2000)28<391:DIAAPC>2.0.CO;2.

Osinski, G. R., et al. (2011), Impact ejecta emplacement on terrestrial planets, *Earth Planet. Sci. Lett.*, *310*(3–4), 167–181, doi:10.1016/j.epsl.2011.08.012.

Pedersen, G. B. M., et al. (2010), Formation, erosion and exposure of Early Amazonian dikes, dike swarms and possible subglacial eruptions in the Elysium Rise/Utopia Basin region, Mars, *Earth Planet. Sci. Lett.*, *294*(3–4), 424–439, doi:10.1016/j.epsl.2009.08.010.

Pelkey, S. M., et al. (2007), CRISM multispectral summary products: Parameterizing mineral diversity on Mars from reflectance, *J. Geophys. Res.*, *112*, E08S14, doi:10.1029/2006JE002831.

Ray, R., et al. (2007), Structure and emplacement of the Nandurbar-Dhule mafic dyke swarm, Deccan Traps, and the tectonomagmatic evolution of flood basalts, *Bull. Volcanol.*, *69*(5), 537–551, doi:10.1007/s00445-006-0089-y.

Rubin, A. M. (1992), Dike-induced faulting and graben subsidence in volcanic rift zones, *J. Geophys. Res.*, *97*(B2), 1839–1858, doi:10.1029/91JB02170.

Salvatore, M. R., J. F. Mustard, M. B. Wyatt, and S. L. Murchie (2010), Definitive evidence of Hesperian basalt in Acidalia and Chryse planitiae, *J. Geophys. Res.*, *115*, E07005, doi:10.1029/2009JE003519.

Schultz, R. A., et al. (2004), Igneous dikes on Mars revealed by Mars Orbiter Laser Altimeter topography, *Geology*, *32*(10), 889–892, doi:10.1130/G20548.1.

Shean, D. E., J. W. Head, and D. R. Marchant (2005), Origin and evolution of a cold-based tropical mountain glacier on Mars: The Pavonis Mons

fan-shaped deposit, *J. Geophys. Res.*, *110*, E05001,doi:10.1029/2004JE002360.

Werner, S. C. (2009), The global Martian volcanic evolutionary history, *Icarus*, *201*(1), 44–68, doi:10.1016/j.icarus.2008.12.019.

Wilson, L., and J. W. Head (1988), Nature of local magma storage zones and geometry of conduit systems below basaltic eruption sites: Pu'u 'O'o, Kilauea East Rift, Hawaii, example, *J. Geophys. Res.*, *93*(B12), 14,785–14,792, doi:10.1029/JB093iB12p14785.

Wilson, L., and J. W. Head (2002), Tharsis-radial graben systems as the surface manifestation of plume-related dike intrusion complexes: Models and implications, *J. Geophys. Res.*, *107*(E8), 5057, doi:10.1029/2001JE001593.

Xiao, L., et al. (2012), Ancient volcanism and its implication for thermal evolution of Mars, *Earth Planet. Sci. Lett.*, *323–324*, 9–18, doi:10.1016/j.epsl.2012.01.027.